JOURNAL OF NEUROTRAUMA 29:499–513 (February 10, 2012)

DOI: 10.1089/neu.2011.2076

Chronic Spinal Compression Model in Minipigs: A Systematic Behavioral, Qualitative, and Quantitative Neuropathological Study

Roman Navarro,[1] Stefan Juhas,[2] Sassan Keshavarzi,[3] Jana Juhasova,[2] Jan Motlik,[2] Karl Johe,[4] Silvia Marsala,[1] Miriam Scadeng,[5] Peter Lazar,[6] Zoltan Tomori,[7] Gery Schulteis,[8] Michael Beattie,[9] Joseph D. Ciacci,[3] and Martin Marsala[1]

Abstract

The goal of the present study was to develop a porcine spinal cord injury (SCI) model, and to describe the neurological outcome and characterize the corresponding quantitative and qualitative histological changes at 4–9 months after injury. Adult Gottingen-Minnesota minipigs were anesthetized and placed in a spine immobilization frame. The exposed T12 spinal segment was compressed in a dorso-ventral direction using a 5-mm-diameter circular bar with a progressively increasing peak force (1.5, 2.0, or 2.5 kg) at a velocity of 3 cm/sec. During recovery, motor and sensory function were periodically monitored. After survival, the animals were perfusion fixed and the extent of local SCI was analyzed by (1) post-mortem MRI analysis of dissected spinal cords, (2) qualitative and quantitative analysis of axonal survival at the epicenter of injury, and (3) defining the presence of local inflammatory changes, astrocytosis, and schwannosis. Following 2.5-kg spinal cord compression the animals demonstrated a near complete loss of motor and sensory function with no recovery over the next 4–9 months. Those that underwent spinal cord compression with 2 kg force developed an incomplete injury with progressive partial neurological recovery characterized by a restricted ability to stand and walk. Animals injured with a spinal compression force of 1.5 kg showed near normal ambulation 10 days after injury. In fully paralyzed animals (2.5 kg), MRI analysis demonstrated a loss of spinal white matter integrity and extensive septal cavitations. A significant correlation between the magnitude of loss of small and medium-sized myelinated axons in the ventral funiculus and neurological deficits was identified. These data, demonstrating stable neurological deficits in severely injured animals, similarities of spinal pathology to humans, and relatively good post-injury tolerance of this strain of minipigs to spinal trauma, suggest that this model can successfully be used to study therapeutic interventions targeting both acute and chronic stages of SCI.

Key words: axonal loss; chronic spinal injury; minipig; paraplegia

Introduction

There is a need for large animal models of spinal cord injury (SCI) with qualitative and quantitative neurological dysfunction and spinal cord histopathology comparable to those of human patients. These models would allow for further characterization of the pathophysiology of SCI and validation of potentially effective therapies.

Currently available animal models of SCI are characterized by the animal species employed and the mechanism by which the spinal trauma is induced (weight drop, contusion, calibrated forceps compression, or laceration). The power of any model in determining the clinical relevance of a therapy is determined by: (1) how similar the model is to the clinical and histopathological picture of human SCI, (2) the reproducibility of neurological dysfunction across individual

[1]Neuroregeneration Laboratory, Department of Anesthesiology, [3]Division of Neurosurgery, and [5]Center for Functional MRI, University of California, San Diego (UCSD), San Diego, California.
[2]Institute of Animal Physiology and Genetics, Czech Academy of Sciences, Libechov, Czech Republic.
[4]Neuralstem, Inc., Rockville, Maryland.
[6]University of Veterinary Medicine and Pharmacy, Department of Breeding and Diseases of Game and Fish, Kosice, Slovakia.
[7]Institute of Experimental Physics, SAS, Kosice, Slovakia.
[8]Research Service, VA San Diego Healthcare System and Department of Anesthesiology, UCSD School of Medicine, San Diego, California.
[9]Brain and Spinal Injury Center, Department of Neurological Surgery, University of California, San Francisco, San Francisco, California.

experimental subjects exposed to an identical injury, (3) the degree and the time course of spontaneous motor/sensory recovery, (4) tolerability to chronic neurological dysfunction and related post-injury animal care, (5) the capability of generating different degrees of functional outcome after different severities of injury, and (6) the ability to qualitatively and quantitatively describe the spinal histopathological changes.

The rodent (mouse and rat) models of SCI are widely used. Rodents were originally selected because the functional, biochemical, and morphological changes of SCI were thought to be similar to those in humans. Using rat models of spinal contusion, weight-drop, or epidural balloon-compression-induced injury, a correlation between the degree of neurological deficit (as measured by the Basso-Beattie-Bresnahan [BBB] or Combined Behavioral Score [CBS]) and the extent of local tissue degeneration at the injury epicenter has been reported in numerous studies and independently validated in several laboratories (Basso et al., 1996b; Noble and Wrathall, 1989; Vanicky et al., 2001). However, interestingly, even after severe spinal cord injury characterized by 85–95% of axonal loss or overall tissue degeneration, progressive recovery is seen over a 3- to 6-week period after injury, with the average BBB score ranging between 6 and 11 in both T10 contusion and weight-drop models in rats (Basso et al., 1996a; Ek et al., 2010; Fischer and Peduzzi, 2007). The mechanism of this spontaneous recovery is not clear, but progressive remyelination and axonal sprouting from the remaining brainstem-derived descending motor axons below the injury may in part account for this effect (Curtis et al., 1993; Salgado-Ceballos et al., 1998). More importantly, such a high degree of spontaneous recovery represents a significant challenge in detecting relevant clinical benefit from the various therapeutic strategies examined. Preclinical and clinical data demonstrate that so far none of the therapies with promising outcomes in mouse or rat models have been effective in human patients (Hawryluk et al., 2008; Tator, 2006). Such a differential responsivity between rodents and humans to a given treatment may reflect differences in the pathophysiology of spinal cord injury, and/or our inadequate understanding of the interventional limitations when directly translated from rodents to man (Dietz and Curt, 2006; Hagg and Oudega, 2006; Tator, 2006). A recent survey of 324 members of the SCI community reported strong support for first demonstrating the efficacy of various therapies in large-animal models (in addition to rodent models), as well as independent replication of promising results before moving forward with human clinical trials (Kwon et al., 2010).

In comparison to rodents, there are relatively fewer experimental studies that have employed large-animal models of SCI (Akhtar et al., 2008; Kuluz et al., 2010; Lim et al., 2010). Limitations of developing and conducting large-scale studies that would employ large-animal models of SCI include: (1) the complexity of post-injury animal care and management of complications associated with complete or incomplete loss of motor function (e.g., bladder infection, skin ulcers, or gastrointestinal complications), (2) the required expertise in large-animal surgery, and (3) the financial cost associated with large-animal studies.

Early studies have employed weight-drop or epidural-balloon-compression technique to induce spinal injury in dogs. While no systematic axonal quantification was performed in those studies, the development of extensive local tissue cavitations and loss of gray and white matter integrity at the injury site was seen in animals after severe trauma. These histopathological changes corresponded with stable neurological deficits (paralysis), which persisted up to 3 months after injury (Allen, 1911; Tarlov, 1954; Tarlov and Klinger, 1954). In a more recent study, a similar epidural-balloon-compression model as described by Tarlov (Tarlov, 1954) has been reported in dogs (Fukuda et al., 2005). Using MRI-measured lesion volume, a correlation between the loss of neurological function and the extent of local tissue injury was demonstrated. Similarly, as seen in the early studies, no spontaneous recovery was noted for up to 6 months after severe spinal trauma. In contrast to the dog model of spinal injury, a much higher functional recovery rate was reported in the cat. After using weight-drop to create a severe contusion injury in the mid-thoracic (T7–T8) spinal cord, it was demonstrated that some animals had recovery of effective locomotion 4–8 months after injury, with only 5–10% axonal survival (Blight, 1983; Blight and Decrescito, 1986).

Progressive axonal degeneration has been described in rhesus monkeys following graded dorsal spinal cord impact injury of 200, 300, 400, or 500 g/cm (Bresnahan, 1976,1978). More recently a graded cervical contusion injury model (using weight-drop injury of the C5 segment) in non-human primates (common marmoset) was developed. In this model the degree of motor performance correlated with the loss of myelinated areas at and around the injury epicenter with relatively stable deficits seen 10 weeks after injury (Iwanami et al., 2005).

Thus it is apparent that even after using large-animal species to induce spinal cord injury, a different degree of spontaneous recovery can be expected, depending on the animal species employed, the mechanism of how the injury is induced, and the spinal level targeted. This also suggests that a detailed morphometric analysis (axonal counts) in specific spinal cord regions (funiculi), and correlative neurological assessments at different stages after injury, need to be conducted to define the optimal large-animal model of spinal trauma that would parallel at least some aspects of human SCI pathology and neurological dysfunction.

In this study, we characterize a chronic spinal contusion model in adult Gottingen-Minnesota (GM) minipigs. The primary goal was to demonstrate: (1) a correlation between the degree of neurological dysfunction and axonal loss at the epicenter of the injured T12 spinal segment, (2) the time course and stability of neurological dysfunction seen after graded spinal cord contusion, (3) the degree of rostrocaudal cavitation (i.e., syringomyelia), and (4) long-term (9 months) tolerability of animals to partial or severe neurological dysfunction (paraplegia).

Methods

These studies were carried out under protocols approved by the Institutional Animal Care and Use Committee of the Czech Academy of Sciences, and were in compliance with Association for Assessment of Laboratory Animal Care guidelines for animal use. All studies were performed in such a manner as to minimize group size and animal suffering.

General animal preparation

Minipigs resulting from Minnesota, Gottingen, and domestic farm (Libechov) strain cross-breeding (both sexes;

18–23 kg; $n = 21$; 12 females and 9 males) were premedicated with intramuscular azaperone (2 mg/kg) and atropine (1 mg/kg), and then induced with ketamine (20 mg/kg IV). After induction, the animals were intubated with a 2.5-F tracheal tube. Anesthesia was maintained with a 1.5% isoflurane in 50/50% air-oxygen mixture at a constant 2 L/min flow rate. Oxygen saturation was monitored throughout the procedure using a pulse oximeter (Nellcor Puritan Bennett Inc., Galway, Ireland). After induction of anesthesia, the animals were placed in a spinal immobilization apparatus consisting of a stainless steel platform (20×35″), four vertical bars (2×2″ and 15″ tall), and four horizontal bars. To achieve immobilization of the lower thoracic and lumbar spine, the lumbar portion of the animal was lifted 5″ above the operating table and 4 horizontal bars were slid bilaterally against the lateral portion of the vertebral column just ventral to the L1–L4 paravertebral muscle. The skin was left intact. Dorsal laminectomy of the T11–T13 vertebrae exposing the T12 spinal segment was then performed. Epidural fat was removed using cotton swabs. The dura was left intact. Dorso-ventral compression of the T12 segment was then induced using a computer-controlled spinal compression apparatus consisting of a stepping motor (IMS-17; Intelligent Motion Systems, Marlborough, CT), and a vertically-oriented digital force gauge (0–5 kg range; Omega Engineering Inc., Stamford, CT) bridged to an aluminum rod 5 mm in diameter (Fig. 1A). Compression device-controlling software FORCE (ViDiTo, Kosice, Slovakia) permits preprogramming of variable compression parameters, including maximum compression pressure, velocity of compression, and duration of compression. The compression curve was recorded in each individual animal to assure consistency of compression parameters across animals (Fig. 1B, C, and D). Just before compression, the animals were injected with succinylcholine (125 mg IV; VUAB Pharma, Roztoky, Czech Republic) to induce muscle relaxation. After compression, the surgical incisions were closed in anatomical layers and the animals were allowed to recover. All animals were treated with gentamicin (2 mg/kg/day IM) for the initial 14 days after spinal trauma.

Experimental groups

Three experimental groups were studied with compression pressure cut-off set at 1.5 kg (group A, $n = 6$; Fig. 1B), 2 kg (group B, $n = 7$; Fig. 1C), or 2.5 kg (group C, $n = 8$; Fig. 1D), and delivered at a velocity of 3 cm/sec. The animals were allowed to survive for 4 or 9 months ($n = 3$–4 for each time point and compression group).

Neurological assessment

Motor function. Recovery of motor function was assessed using a 14-point scoring system (porcine neurological motor score [PNM score]; Table 1). This system was designed to permit the assessment of (1) movement in all three joints in the lower extremities and tail, with no weight support, and (2) the degree of recovery of ambulatory function, with weight support.

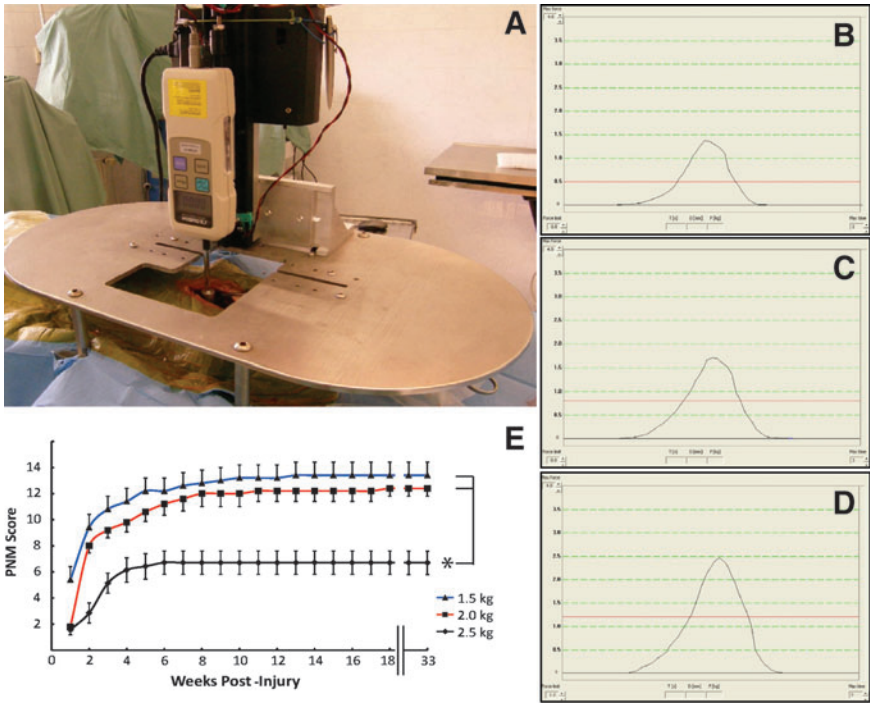

FIG. 1. (**A**) To compress the exposed spinal cord, a spinal compression apparatus consisting of a computer-controlled stepping motor and digital force transducer is mounted on the top of the metal platform and positioned just above the exposed T12 spinal segment. (**B**–**D**) A compression curve is recorded in each animal just before, during, and after compression, and the consistency of compression parameters is validated. A typical compression curve recording pattern in an animal after 1.5 kg (**B**), 2.0 kg (**C**), and 2.5 kg (**D**) compression. (**E**) Porcine neurological motor score (PNM score) in animals in all three compression groups during the 9 months of survival after spinal trauma. Compression magnitude-dependent loss of ambulatory function can be seen (0 = complete loss of motor function; 14 = normal ambulatory function; $^*p < 0.01$ by repeated-measures analysis of variance). Color image is available online at www.liebertonline.com/neu

Table 1. Porcine Neurological Motor Score (PNM) Score

Grade 0: complete paraplegia; no movement in both lower limbs; no tail movement
Grade 1: slight movement in one or two joints in one lower limb; no tail movement
Grade 2: slight movement in one or two joints in one lower limb; tail movement present
Grade 3: extensive movement of all three joints in one hindlimb; no tail movement
Grade 4: extensive movement of all three joints in one hindlimb; tail movement present
Grade 5: slight movement in one or two joints of both hindlimbs; no tail movement
Grade 6: slight movement in one or two joints of both hindlimbs; tail movement present
Grade 7: extensive movement in all three joints of both hindlimbs; no tail movement
Grade 8: extensive movement in all three joints of both hindlimbs; not able to bear weight even if initially helped to stand; tail movement present
Grade 9: plantar-hoof support with weight bearing only if helped to stand; not able to take any steps; tail movement present
Grade 10: capable of standing up on its own; able to take 1–-3 steps before losing balance; prevalence of dorsal-hoof stepping; tail movement present
Grade 11: capable of standing up spontaneously; able to take 3–5 steps; can keep balance between stepping episodes; occasional plantar-hoof stepping; tail movement present
Grade 12: capable of standing up spontaneously with sustained locomotion for 5–10 steps; occasional to frequent plantar-hoof stepping; no or inconsistent forelimb-hindlimb coordination; tail movement present
Grade 13: capable of standing up spontaneously on hindlimbs with sustained locomotion for more than 10 steps; frequent plantar-hoof stepping; frequent forelimb-hindlimb coordination; not able to pass hindlimb clearance test;[a] tail movement present
Grade 14: capable of standing up spontaneously on hindlimbs with sustained locomotion; consistent plantar-hoof stepping; consistent forelimb-hindlimb coordination; able to pass hindlimb clearance test; tail movement present

[a]Hindlimb clearance test: Testing of hindlimb clearance was only performed in animals with neurological scores of 13 or 14 to discriminate forelimb-hindlimb coordination in more detail. To perform this test, the animals are guided to step over a 4×4″ wooden bar in an open field. A normal animal typically shows complete clearance without touching the bar. Failure to pass this test is assigned when the animal is not able to step over the bar, or if it touches the bar during clearance attempts in 3 consecutive tests.

Testing of motor function during the entire course of the study was performed by two investigators who were also involved in the development of the neurological scoring system (S.J. and J.J.). The variability in the scores between the two raters was typically 1–2 points. To minimize the variability, a video was captured weekly for all animals during the first month post-injury, and any discrepancies in the scores obtained by the two raters were retrospectively discussed and clarified while comparing with specific video footage. From our experience, the 1-month neurological scoring training session was sufficient to minimize inter-rater differences.

Sensory function. Sensory function was assessed by the presence of the withdrawal response to a mechanical stimulus. The toes of the front- and hindlimbs were progressively compressed with Halsted forceps. Typically, partial application of forceps would evoke a vigorous withdrawal response or vocalization, and the stimulus was stopped immediately. The response was scored as present or absent.

Measurement of allodynia. The presence of allodynia was assessed by applying a brief, non-noxious stimuli to the lower back and both lower extremities by compressing the skin with a 0.5-cm-diameter aluminum bar bridged to a digital pressure meter. Pressure cut-off was set at 0.5 kg and was based on our preliminary study in control animals that showed no responsiveness at this compression pressure. Animal vocalization or a clearly detectable muscle twitch seen immediately after application of the stimulus was considered to be a positive response.

Anal sensation. Anal sensation was assessed using an electric von Frey hair (2393 Series Electronic von Frey Anesthesiometer; IITC Life Science Inc., Woodland Hills, CA). The response (contraction of the anal sphincter) was scored as present or absent.

Muscle hypertonia and stimulus-evoked muscle hyperreflexia. The presence of muscle hypertonia was defined as a spontaneous (stimulus-independent) increase in muscle tone. A positive response was assigned when the partially or fully paralyzed extremity was extended or flexed in the knee or hip joint, and returned to its original position.

The presence of muscle hyperreflexia was defined as exacerbated muscle contractions in the lower extremity after applying a skin nociceptive stimulus at the level of the gastrocnemius muscle. Skin was progressively compressed with Halsted forceps until a clear withdrawal response or spinal reflex-mediated muscle contraction (in paraplegic animals) was seen. Continuing muscle contraction lasting for more than 2 sec was considered as a positive hyperreflexia response.

Perfusion fixation and preparation of spinal cord tissue for sectioning

At the end of survival, the animals were deeply anesthetized with pentobarbital (100 mg/kg) and transcardially perfused with heparinized saline (4 U/mL; 5 L), followed by 5 L of 4% paraformaldehyde in 0.1 M phosphate buffer (pH 7.4), or with 5 L of a 4% paraformaldehyde/0.3% glutaraldehyde mixture in 0.1 M phosphate buffer (pH 7.4). Spinal cords were dissected from the vertebral column and post-fixed overnight at 4°C. After dissection, the spinal cords were macroscopically examined for identification of the injury and imaged by magnetic resonance imaging (MRI) before sectioning. After MRI, the spinal cords were sectioned into 2- to 3-mm coronal blocks. For spatial orientation, rostral segments were assigned

positive increasing integers, and caudal segments were assigned negative increasing integers. The injury epicenter was assigned a value of 0. Spinal blocks containing the injury epicenter were further post-fixed in 0.3% glutaraldehyde in 0.1 M PBS (pH 7.4) overnight at 4°C in preparation for plastic embedding. All other tissue blocks were cryoprotected in 30% sucrose with 0.02% sodium azide and used for cryosectioning and immunostaining.

Post-mortem magnetic resonance imaging

The excised minipig spinal cords were image immersed in perfluorocarbon. Images were acquired in a horizontal bore 7-T MRI (GE Medical Systems, Milwaukee, WI), with a 10-mm transmit/receive MR imaging surface coil using a 2D FSPGR sequence (TR/TE = 10/2.9, FA = 20°, FOV = 10 mm, matrix 160 × 128, and slice thickness = 100 microns). Imaging time was 60 min.

Three-dimensional rendering and anatomical measurements. The image data sets were manually volume- and surface-rendered using AMIRA software (Mercury Computer Systems, Chelmsford, MA) to produce quantitative three-dimensional models. From these computed models, dimensions such as cavity volume and surface area at the injury site can be determined.

Immunofluorescence and immunohistochemical staining

Transverse (20- to 30-μm-thick) spinal cord sections prepared from spinal cord regions just rostral and caudal to the injury epicenter (designated as +1 and −1) were used. For immunofluorescence staining, tissue from 4% paraformaldehyde-perfused animals was used. Because of intense autofluorescence in glutaraldehyde-fixed spinal cords, these sections were developed using an avidin/biotin horseradish peroxidase immunohistochemical protocol.

For immunofluorescence staining, sections were incubated with the following primary antibodies in 0.2% Triton-X 100 (TX) overnight at 4°C: rabbit anti-glial fibrillary acidic protein (GFAP, 1:1000; Chemicon, Temecula, CA), mouse anti-neurofilament (NF, 1:1000, SMI-312; Covance, Princeton, NJ), rabbit anti-IBA-1 (1:1000; Wako, Richmond, VA), and mouse anti-Schwann/2E (1:1000; Cosmo Bios Co., Ltd., Tokyo, Japan). Following washing in PBS 3 × 5 min, the sections were incubated with goat or donkey secondary fluorescent antibodies (1:250, Alexa-Fluor 488 or 594; Millipore, Billerica, MA) for 1 h at room temperature. For general nuclear staining, 4′,6′,-diamidino-2-phenylindole (DAPI, 1:250) was added to all secondary antibody solutions. Images of fluorescent sections (1024 × 1024 pixels) were captured with an Olympus Fluoview FV1000 confocal microscope with a 20 × objective/0.75 numerical aperture, optical section spacing of 0.5 μm, and pulse speed of 20 μsec/pixel.

For immunohistochemical staining, the sections were first treated in 1% sodium borohydride for 30 min, followed by washing in PBS 3 × 3 min. The sections were then placed in 3% H_2O_2 for 15 min, and washed 3 × 3 min in PBS. Preincubation to suppress non-specific protein activity was performed using 5% goat or rabbit serum, 0.2% TX, and 0.2% bovine serum albumin in PBS for 1 h. The sections were then incubated with the following primary antibodies: rabbit anti-GFAP (1:1000), mouse anti-neurofilament (1:1000), and rabbit anti-IBA-1 (1:1000), in 5% goat or rabbit serum in PBS overnight at 4°C. After incubation with primary antibodies, the sections were washed in PBS 3 × 3 min and incubated with biotinylated goat or rabbit secondary (1:250) antibodies for 1 h. Bound specific antibodies were reacted with the avidin-biotin peroxidase solution for 1 h, and then visualized using a 3,3,4,4-diaminobezidine hydrochloride (DAB)-peroxidase substrate kit (Vector Laboratories Inc., Burlingame, CA). Brightfield images of DAB-stained sections were captured using a Leica DMLB Microscope with a 40 × objective using an Olympus Firewire camera.

Tissue processing for plastic embedding and semi-thin sectioning

Spinal cord blocks (2 to 3 mm thick) taken from the injury epicenter were used for plastic embedding. Following post-fixation in 0.3% glutaraldehyde for 1 day at 4°C, the tissues were rinsed 3 × 5 min in PBS and stored in PBS overnight at 4°C. Secondary post-fixation was performed using 0.1% osmium tetroxide in 0.1 M non-saline phosphate buffer (pH 7.4) for 12 h, followed by adequate rinsing in non-saline phosphate buffer. This was followed by progressive alcohol dehydration according to standard procedures up to 100% ethanol, with the addition of further dehydration in a 1:1 solution of ethanol/propylene oxide, and lastly 100% propylene oxide. Dehydrated blocks were then prepared for resin infiltration by incubation in a 1:1 solution of resin/propylene oxide on a rotator in a fume hood overnight. The resin solution used consisted of: Eponate 12, Araldite 502, dodecenyl succinic anhydride (DDSA), and 2,4,6-tri [dimethylaminomethyl] phenol (DMP-30; Ted Pella, Inc., Redding, CA), mixed in ratios of 10:10:25:1, respectively. The blocks were then transferred to 100% resin for subsequent overnight infiltration on a rotator. Finally, the tissue blocks were embedded using fresh resin in in-house-manufactured multi-chamber silicone rubber molds made with a Silastic® E RVT Silicone Rubber Kit (Dow Corning Corp., Midland Township, MI). This allowed for the entire minipig spinal cord block to be sectioned transversely. The molds with embedded sections were placed in an oven at 60°C for 2 days to facilitate resin polymerization. Semi-thin (1 μm) transverse sections were then cut using a microtome (Leica RM2065 Supercut) with 10-mm glass knives. The sections were mounted on slides with distilled water and allowed to dry on a slide warmer. Prior to staining, the slides were incubated at 60°C in an oven for 10–15 min, and then contrast-stained with 4% para-phenylenediamine (PPD).

Axonal quantification

For axonal quantification, high-resolution mosaic images were obtained from semi-thin sections using a Zeiss Observer system (Z1 microscope system with a 20 × objective fitted with a Zeiss MRm camera, and AxioVision [V 4.7] software with Multidimensional Acquisition MosiaX feature). Images were loaded into Photoshop CS3 to manually remove any non-white matter elements and image format conversion to grayscale. Complete mosaic images were loaded into Image Pro V 6.3. Axonal quantification involved manual definition of pixel threshold (0–255; i.e., values that were held consistent throughout all image analyses). Further measurement

parameters such as area/box and size (length) were applied to discriminate and exclude non-axonal objects. Employment of the size (length) parameter allowed for further axonal analysis, in which axons were divided into empirically-derived caliber sizes of small, medium, and large axons (0.5–2.0 μm, 2.01–10.0 μm, and 10.01–17.0 μm, respectively).

Statistical analysis

Neurological outcome was analyzed using mixed-design ANOVA (group × time post-compression), followed by comparisons of the simple main effects among individual compression groups. A p value of 0.05, Bonferroni-corrected for multiple comparisons, was considered significant. Axonal counting and loss were expressed as mean ± standard error of the mean (SEM), or percentage of baseline control numbers obtained from non-injured animals. The correlation between axonal loss analyzed in the dorsal, lateral, or ventral funiculi, magnitude of compression, and motor deficits, were assessed by second-order polynomial regression.

Results

General animal health and tolerance of graded spinal injury

Animals in all experimental groups survived the spinal cord compression procedure. One male minipig from the 2.5-kg compression group developed urinary retention at 3 weeks post-trauma. Repetitive attempts to perform Crede's maneuver were not successful and the animal was sacrificed. One female developed anal prolapse at 7 months after injury, which was surgically corrected. After surgery, this animal was treated with antibiotics (Eficur, 3 mg/kg, and Draxxin, 2.5 mg/kg) for 14 days, and then survived for an additional 2 months without further complications. In 2 animals, small-diameter (0.5–1 inch) ulcers developed at 5 and 6 months (2.5-kg compression group) in the ankle joint area and were effectively treated with topical antibiotics and iodide solution. The rest of the animals survived without any complications.

Neurological outcome

Motor function. Assessment of open-field motor function was performed using the 14-point scoring system. Control/complete recovery was defined as grade 14, with the animals capable of spontaneously standing on their hindlimbs with sustained locomotion, consistent hoof stepping, consistent forelimb and hindlimb coordination, and presence of tail movement. These animals also successfully passed a hindlimb clearance test, indicating normal forelimb/hindlimb coordination (Table 1).

Animals in all three compression groups demonstrated unaffected upper extremity function, while a clear compression magnitude-dependent loss of neurological function in the lower extremities was seen across all three experimental groups (Fig. 1E).

The lowest compression group (group A, 1.5 kg) demonstrated a transient deficit (grade 9–11) immediately after injury (5–10 days), followed by nearly complete neurological recovery at 7 weeks post-injury. Three of six animals were not able to pass a hindlimb clearance test 4–9 months after injury.

The medium-compression animals (group B, 2.0 kg) showed a stable, moderate neurological deficit (grade 11–12) 11 weeks after injury, and there was no further improvement for the additional 6 months of survival. These animals were capable of standing spontaneously, completing 3–5 steps while maintaining balance between stepping episodes, and showing occasional plantar-hoof stepping. Tail movement was also present in all animals. Only 1 of 7 animals passed the hindlimb clearance test.

The maximum-compression group (group C, 2.5 kg) showed stable neurological deficits by 5 weeks post-injury (grade 6), and this degree of deficit remained unchanged for the 9 months of survival. These animals were not able to bear weight or stand, even with assistance. Four of eight animals exhibited extensive movement in all three joints of both hindlimbs. In the other four animals, while movement in all three joints was present, it was combined with increased baseline muscle tone (i.e., spastic hypertonia). Tail movement recovered between 4 and 6 weeks in four animals.

A mixed-design ANOVA with time post-compression as a within-subjects factor, and group as a between-subjects factor revealed a significant ($p < 0.001$) main effect of group, main effect of time, and time × group interaction. Follow-up comparisons of the simple main effects of group revealed that the high-compression group (2.5 kg) was different from the 2.0-kg and 1.5-kg group (Bonferroni-corrected $p < 0.05$). The 2.0-kg group and 1.5-kg group were no different from each other.

Sensory function. Analysis of withdrawal response to a mechanical stimulus showed a normal response in all but two animals in the 2.5-kg compression group. No allodynia was detected in any animal. Anal reflex was absent in two animals in the 2.5-kg compression group.

Development of muscle hypertonia and sensory input-evoked muscle hyperreflexia. Four animals that underwent severe trauma (2.5-kg compression group) and showed a baseline increase in muscle tone (i.e., spastic hypertonia), also displayed exacerbated muscle contractions lasting several seconds after applying a skin nociceptive stimulus at the level of the gastrocnemius muscle. This exacerbated response remained unchanged for 4–9 months after injury.

Macroscopic changes in the spinal cord

After dissection of the spinal cord from the spinal column, the presence of previous traumatic injury could easily be identified in all spinal cords by the presence of prominent meningeal fibrosis. Dissection of the dura mater revealed extensive fibrotic adhesions between the dura and underlying spinal cord tissue. These adhesions were only noticed locally at the injury epicenter, and were most extensive in the 2.5-kg compression group.

Magnetic resonance imaging of post-mortem spinal cords

In all compression groups, a trauma-induced region was clearly identified with MRI, and defined by the loss of spinal cord gray matter/white matter integrity, and the appearance of an irregular higher-density tissue mass (red arrow in Fig. 2B). One of the prominent features in the medium- and high-compression groups (2.0 and 2.5 kg) was the presence of septate fluid-filled cysts that extended in a rostrocaudal direction (i.e., syringomyelia). The most extensive cavitation was seen in the 2.5-kg group. Figure 2B and C show an animal

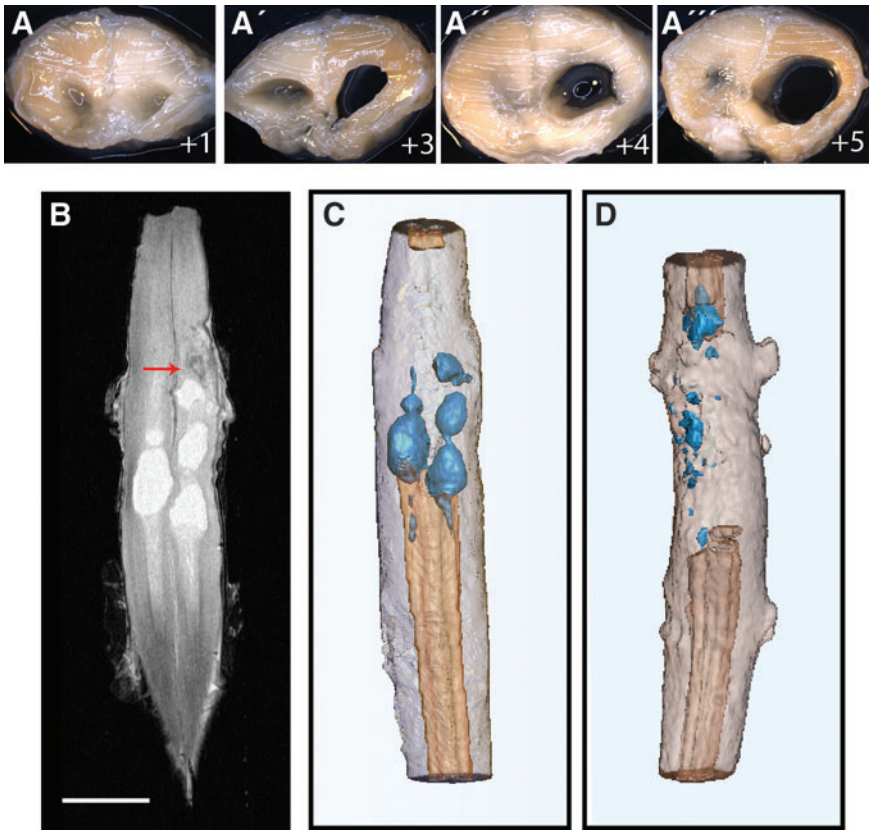

FIG. 2. (**A**–**A‴**) Macroscopic images taken from transversely-sliced spinal cord (thickness of each slice is between 3 and 4 mm) at the injury site in the 2.5-kg compression group with 9 months survival. Extensive bilateral cavities can be identified. Positive integers indicate a location caudal to the injury epicenter (0). (**B**) 2D FSPGR magnetic resonance imaging (MRI) image of the same spinal cord as that seen in **A**–**A‴** confirms the presence of bilateral septic cavitation, and areas of high-density structures around the injury epicenter (red arrow). (**C**) 3D rendered image of the same spinal cord shown in **B**. (**D**) 3D rendered image of another spinal cord in the 2.5-kg compression group showing disseminated smaller cavitations (scale bar in **B** = 8 mm). Color image is available online at www.liebertonline.com/neu

in the 2.5-kg compression group at 9 months after injury, demonstrating bilateral septate cavitations, with some cavities located 2–3 cm caudal to the epicenter of injury. The same spinal cord was then sliced (3- to 4-mm-thick slices), and the presence of cavities verified by visual inspection (Fig. 2A, A′, A″, and A‴). Figure 2D shows the spinal cord from another animal from the 2.5-kg group, demonstrating the presence of disseminated small and medium-sized (1–5 mm in diameter) cavities located rostral and caudal to the epicenter of injury.

Loss of white and gray matter integrity at 4–9 months after injury

Using osmium-treated semi-thin plastic sections taken from the epicenter of injury, a clear loss of spinal cord structure was seen in all compression groups. Depending on the magnitude of compression, several patterns of spinal gray/white matter degeneration and its dorsoventral distribution were noted. First, in the 1.5- and 2.0-kg groups, the major structural loss was noted in the dorsal funiculi (i.e., the site of primary compression), or was seen affecting both dorsal white and gray matter, and in some animals extended unilaterally towards the ventral horn (Fig. 3B–E). We believe the preferential unilateral injury seen in some animals may be the result of partial spinal cord roll-over during the compression. In both groups the gray matter structure was partially preserved, with numerous interneurons and α-motoneurons showing normal structure (Fig. 3J, K, N, O, and P). The affected areas showed a consistent loss of osmium-stained structures, indicating loss of local myelin. In the 2.5-kg group, more advanced changes were noted and were characterized by near complete loss of gray matter structure bilaterally or unilaterally, often replaced by extensive cavities and with partial preservation of lateral and ventral white matter (Fig. 3F–I, L, and M). Comparing the extent of injury between 4 months and 9 months of survival, a comparable degree of white matter and gray matter degeneration was seen. Extensive fibrotic-like tissue masses were also noted at the injury site (Fig. 3Q) in the majority of animals in the 2.5-kg group. We further probed the cellular origin of these structures by staining with Schwann cell-specific (Schwann/2E) antibody. Despite highly specific immunostaining seen at the dorsal root entry zone (to confirm the specificity and cross-reactivity of Schwann/2E antibody with porcine Schwann cells; Fig. 3R), no Schwann/2E immunoreactivity was seen in fibrotic-like tissue. Based on these data and the lack of NF, GFAP, or RIP (2′,3′-cyclic nucleotide 3′-phosphodiesterase antibody; oligodendrocyte marker) staining in these structures (not shown), we speculate that it is primarily composed of fibroblasts (i.e., mesenchymal scar).

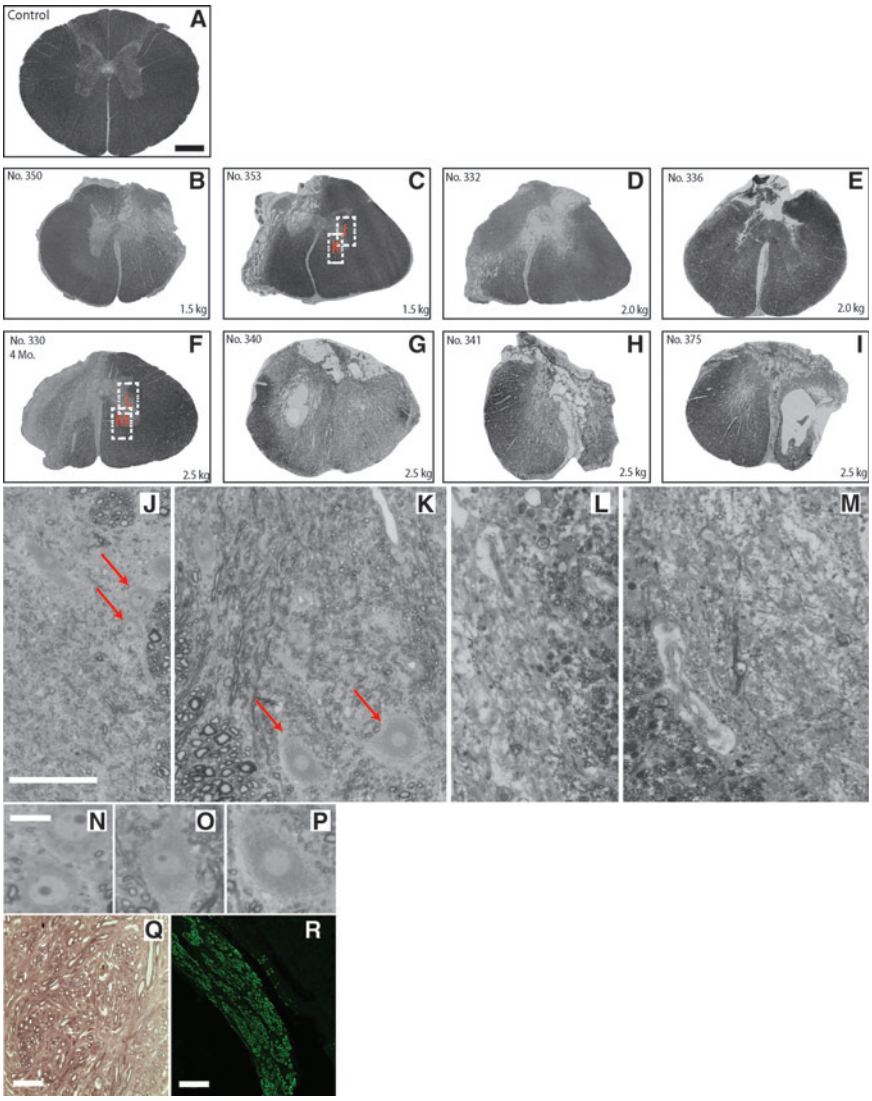

FIG. 3. Examples of mosaic images of the entire plastic cross- section taken from the T12 spinal cord segment of the control (**A**), 1.5-kg compression (**B** and **C**), 2.0-kg compression (**D** and **E**), and 2.5-kg compression (**F–I**) groups. The white dotted boxes in **C** represent areas of the expanded views seen in **J** and **K**, and the white dotted boxes in **F** represent the expanded views seen in **L** and **M** (red arrows in **J** and **K**; **N**, **O**, **P**) after 1.5-kg compression and 4 months survival, numerous normal-appearing α-motoneurons and interneurons located in unaffected areas were identified. (**L** and **M**). In contrast, after 2.5-kg compression, a near-complete loss of α-motoneurons and interneurons in areas with an otherwise normal macroscopic appearance were seen. (**Q**) In some animals fibrotic-like structures were identified in areas adjacent to the injury site at both 4 and 9 months after injury. These structures were negative when stained with Schwann/2E antibody. (**R**) Staining with Schwann/2E antibody showed specific staining of Schwann cells in dorsal roots (scale bars in **A–I** = 1 mm, in **J–M** = 100 μm, in **N**, **O**, and **P** = 60 μm, in **Q** and **R** = 100 μm). Color image is available online at www.liebertonline.com/neu

Qualitative and quantitative analysis of axonal degeneration at 4 and 9 months post-injury

Assessment of axonal loss was performed using Image Pro software by defining intensity threshold and diameter parameters for the objects (axons) to be counted. Examples of the sensitivity of this counting method are demonstrated in Figure 4G and H (images from control and 2.5-kg compression animals at 4 months, respectively). In sections taken from control uninjured animals, the populations of small (0.5–2.0 μm), medium (2.0–10.0 μm), and large (10.0–17.0 μm) myelinated axons are clearly delineated and recognized as individual objects (outlined in red). In contrast, when using the same axon-detection parameters in animals after spinal trauma, a clear loss of axons was readily seen and subsequently confirmed with software-assessed quantification.

Systematic quantitative analysis of the total number of axons counted bilaterally in dorsal, lateral, and ventral funiculi in transverse spinal cord sections taken from the T12 segment in control uninjured animals was 587,884 (Fig. 4A and B). In animals with spinal trauma, a compression-magnitude-dependent loss of axons was seen. The highest-compression group (2.5 kg), the spinal cords showed the greatest overall axonal loss, 83.4% ± 3.2% SEM. In the 2.0-kg

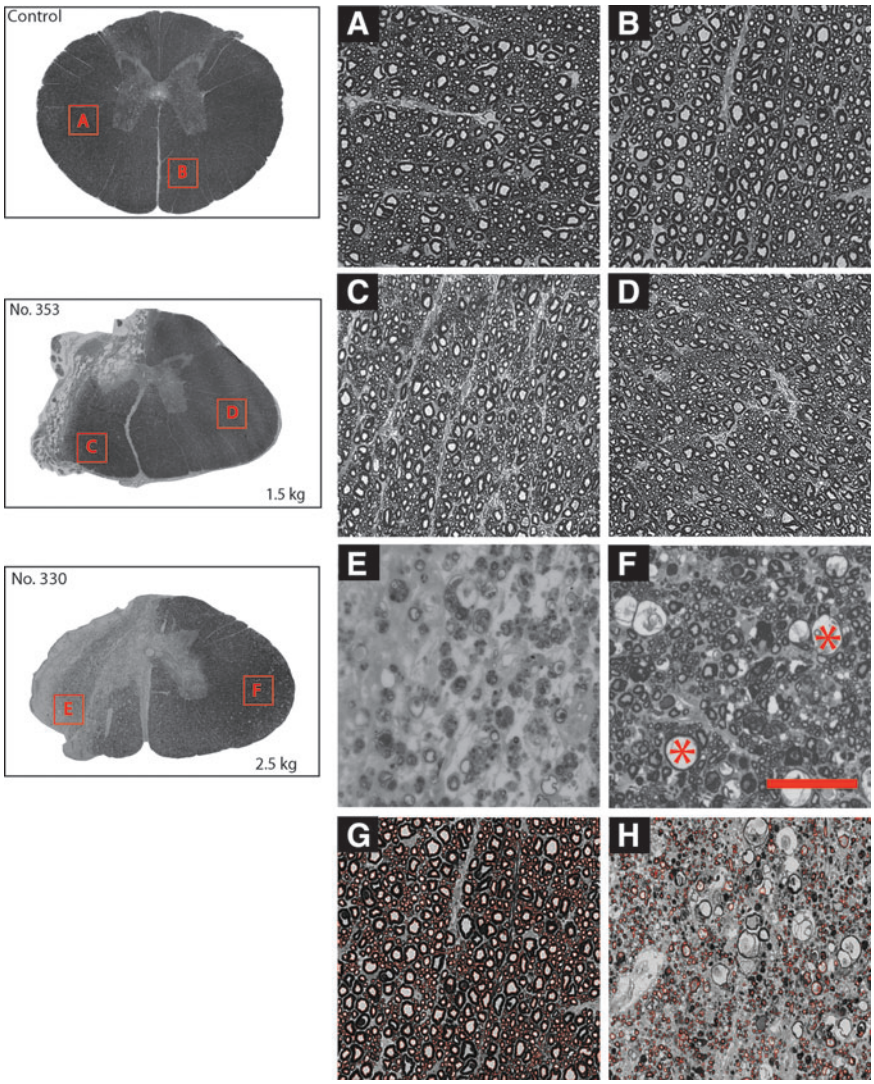

FIG. 4. Microphotographs of cross-sections taken from plastic-embedded T12 segments in control animals and in animals after 1.5 kg and 2.5 kg compression. (**A** and **B**) In control animals, regularly-distributed small-, medium-, and large-caliber myelinated axons in ventral and lateral funiculi can be seen. (**C** and **D**) In animals receiving 1.5-kg spinal compression, a near normal appearance of myelinated axons in areas that were distant from the injury epicenter was seen. (**E** and **F**) In contrast, in animals after 2.5-kg compression, a clear loss of myelinated axons and the presence of vacuolization (red asterisks) was also seen in areas with a near-normal macroscopic appearance, and were distant from the injury epicenter. (**G** and **H**) Examples of the sensitivity of Image Pro software in axonal recognition using digital images taken from plastic transverse spinal cord sections. In control animals, myelinated axons of small, medium, and large caliber can readily be identified (outlined in red). Using the same parameters, a significant loss of myelinated axons can easily be seen in an animal that received 2.5-kg compression and survived for 9 months (scale bars in **A**–**H** = 100 μm). Color image is available online at www.liebertonline.com/neu

compression group, the animals displayed 65.5% ± 1.8% SEM of axonal loss, whereas the 1.5-kg compression group had 30.9% ± 2.0% SEM overall axonal loss.

By comparing the distribution of axonal loss in plastic cross-sections with respect to the epicenter of injury, two specific patterns were noted across all three compression groups. First, in the 1.5- and 2.0-kg groups, axonal loss was identified in the epicenter and areas adjacent to the epicenter of injury. However, only limited white matter degeneration and axonal loss was seen in areas distant from the injury epicenter (Fig. 4C and D). In contrast, in the 2.5-kg group, loss of axons was seen even in areas that were not directly affected by the compression, and had relatively normal anatomic appearance. Numerous large (20–25 μm) cavities were seen in the same areas (red asterisks in Fig. 4F).

Correlative analysis between compression magnitude, axonal loss, and neurological deficits

The sum of overall axonal loss counted in the dorsal, lateral, and ventral funiculi correlated with an R^2 value of 0.984, with compression magnitude measured in individual animals, and an R^2 value of 0.755 with the degree of neurological deficit (Fig. 5A and B). Figure 5C–H demonstrate the relationship between total loss of axons of specific caliber in the dorsal, lateral, or ventral funiculi, and the degree of motor deficit.

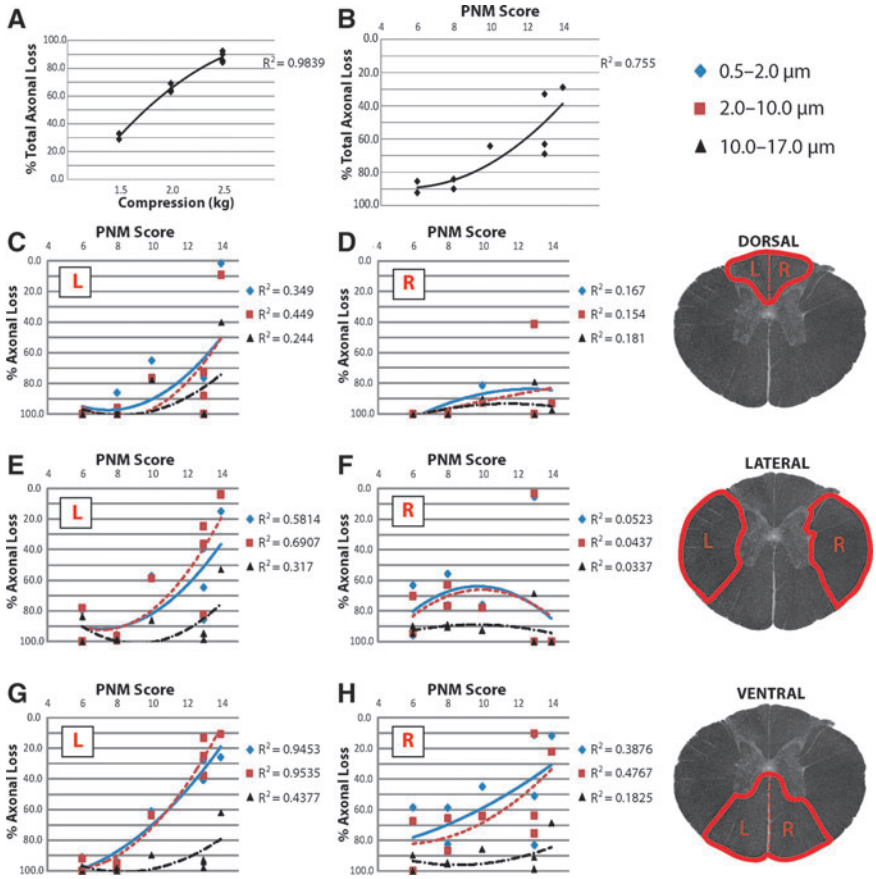

FIG. 5. Correlations between axonal loss quantified bilaterally at the epicenter of injury (T12 segment, **A** and **B**), or in dorsal, lateral, or ventral funiculi (**C**–**H**), with magnitude of compression or the degree of neurological deficits. (**A**) Compression magnitude-dependent axonal loss counted in the entire white matter at the epicenter of injury was seen across all compression groups. (**B**) Correlation between the overall axonal loss and degree of neurological dysfunction (porcine neurological motor [PNM] score) showed that animals with more than 73% axonal loss were non-ambulatory. (**C**–**H**) Correlative analysis between axonal loss quantified in dorsal, lateral, or ventral funiculi, and degree of neurological dysfunction (PNM score), demonstrated the highest degree of correlation with the loss of small- and medium-caliber axons in the ventral funiculi (**G** and **H**). Color image is available online at www.liebertonline.com/neu

The highest correlation was observed between the extent of axonal loss of small (0.5–2.0 μm)- and medium (2.01–10.0 μm)-sized axons in the ventral funiculus and loss of neurological function (Fig. 5G and H).

Qualitative histopathological changes in the spinal cord after injury

4 months. Immunofluorescence analysis of transverse spinal cord sections taken from injured spinal cords (2.5-kg compression group) just above or below the epicenter of injury (Fig. 6E–H and M–P) revealed several pathological patterns. First, in the white matter regions, staining with GFAP antibody demonstrated the presence of regularly-distributed hypertrophic astrocytes surrounding numerous circular cavities (compare Fig. 6A to E). Based on the regular distribution and the diameter of these cavities (20–25 μm), as well as the loss of neurofilament staining in the same areas (Fig. 6M), we speculate that these cavities were primarily formed by a progressive degeneration of injured axons and loss of myelin. Staining of the same sections with IBA-1 antibody revealed an intense infiltration/activation with microglia/macrophages, that corresponded with a clear cellular hyperplasia as defined by increased DAPI staining (compare Fig. 6B–D to F–H). Numerous IBA-1-positive elements were also identified at the borders and at the epicenter of astrocyte-surrounded cavities (Fig. 6G and H). Staining with NF antibody confirmed the loss of an otherwise regular distribution of NF-positive axons in areas heavily infiltrated with IBA-1-positive cells (compare Fig. 6I–L to M–P).

9 months. Immunohistochemical staining 9 months after injury (2.0- and 2.5-kg groups) demonstrates a similar pattern to the staining seen 4 months after injury. Staining with GFAP antibody showed the presence of GFAP-positive hypertrophic processes encapsulating numerous cavities present in the white matter (Fig. 7D and G). In the 1.5-kg group there was a relatively unaffected neuropil and near-normal GFAP staining pattern contralateral to the injury site. In these cases, astrogliosis was anisomorphic in nature (data not shown). Some spinal cords in the 2.5-kg compression group had astrocytic processes that were pilocytic in morphology (Fig. 7G). A typical astrocytic scar that would form a solid scar-forming structure was not identified in any of the animals in the 2.5- or

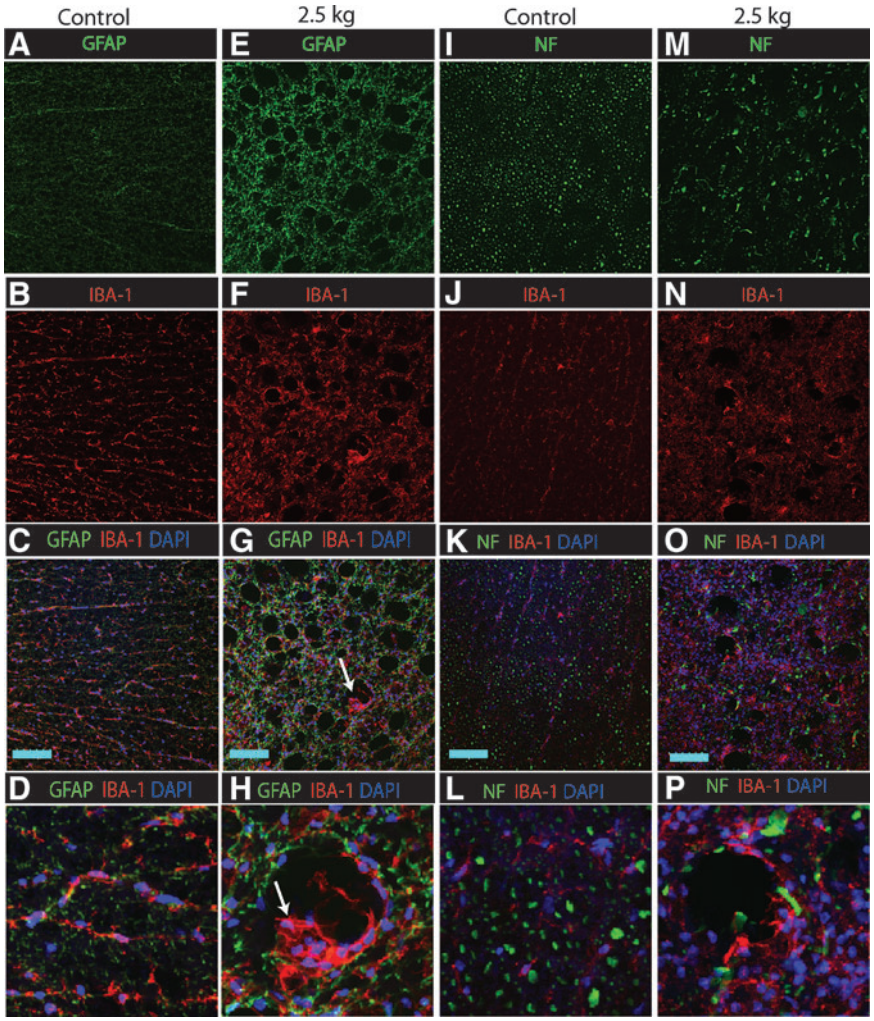

FIG. 6. Confocal images from immunofluorescence-stained transverse spinal cord sections taken from the T12 segment of a control animal (**A**–**D** and **I**–**L**), or from areas just above the injury epicenter in an animal after 2.5-kg compression and 4 months survival (**E**–**H** and **M**–**P**). In animal after trauma, staining with glial fibrillary acidic protein (GFAP) and IBA-1 antibody showed the presence of hypertrophic astrocytes surrounding numerous large-diameter cavities in the lateral white matter (**E**). In the same areas, high-density sequestered IBA-1-positive macrophages/microglia infiltrating astrocyte-surrounded cavities can also be identified (**F** and white arrows in **G** and **H**). Staining with neurofilament antibody (NF, green) showed a clear loss of transversely-cut NF profiles that was particularly pronounced in areas infiltrated by activated microglia and macrophages, and characterized by general cellular hyperplasia (**M**, **N**, **O**, and **P**; scale bars = 100 μm). Color image is available online at www.liebertonline.com/neu

2.0-kg compression groups. Staining with IBA-1 antibody revealed continuing and intense inflammatory activity, with numerous IBA-1-positive cells (Fig. 7E and H). In general, activated microglia/macrophages could be identified in all injury groups, but the intensity of staining was most pronounced in the areas close to the injury epicenter, and was most intense in the 2.5-kg compression group. Staining with NF antibody confirmed a clear loss of NF-positive axons compared to controls (compare Fig. 7C to F and I), and the pattern of NF-positive staining was almost identical to that seen at 4 months.

Discussion

Stable neurological deficit after calibrated spinal cord injury in minipigs

Utilizing a computer-controlled compression apparatus, peak compression forces of 1.5, 2.0, or 2.5 kg were delivered to the surface of the exposed T12 segment at a velocity of 3 cm/sec to induce spinal cord injury in minipigs. The animals in the moderate-compression group (2.0 kg) displayed a loss of ambulatory function for 11 days after they underwent spinal injury. However, over the ensuing 9 months of recovery they progressed to stand and walk. Persisting deficits were characterized by the lack of consistent plantar hoof-stepping, and in the majority of animals, the inability to pass the hindlimb clearance test. In contrast to the moderate-compression group, animals exposed to severe compression (2.5 kg) injury displayed consistent paraplegia with an inability to stand up spontaneously or with assistance. These animals did not recover their motor function qualitatively or quantitatively over the 9-month recovery period. In accordance with prior reports of severe SCI in dogs (Fukuda et al., 2005; Tarlov, 1954), this confirms that in the minipig model a severe trauma produces comparable stable neurological dysfunction, and the degree

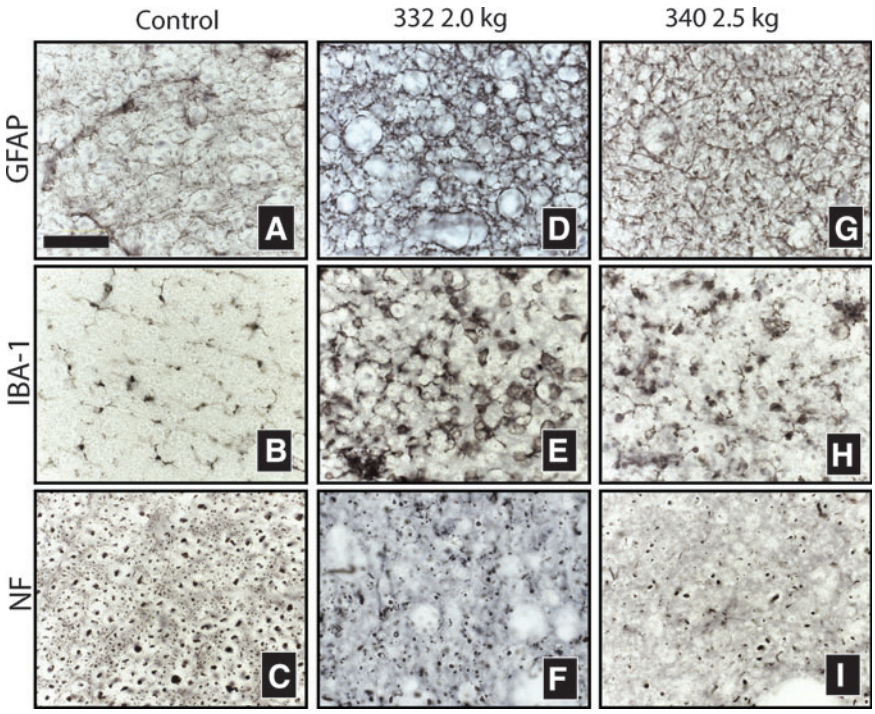

FIG. 7. Brightfield images from immunohistochemically-stained transverse spinal cord sections taken from the T12 segment of a control animal (**A–C**), or from areas just above the injury epicenter in an animal after 2.0-kg and 2.5-kg compression at 9 months of survival (**D–F** and **G–I**; glutaraldehyde-fixed material). In comparison to control tissues, staining with glial fibrillary acidic protein (GFAP) antibody revealed the continuing presence of numerous cavities surrounded by partially hypertrophic pilocytic astrocytes (**D** and **G**). Similarly to the pattern seen at 4 months after injury in the same areas, the continuing presence of high-density activated microglia and macrophages (**E** and **H**), and disintegration of neurofilament (NF)-stained profiles (**F** and **I**) was also seen (scale bar = 100 μm). Color image is available online at www.liebertonline.com/neu

of spontaneous recovery is limited. The recovery is characterized by only modest improvement of movement in affected extremities, but with a persisting presence of functionally defined paraplegia (i.e., inability of the animals to stand and bear weight).

Development of syringomyelia at 9 months after spinal injury

In animals undergoing 2.5-kg compression surviving 9 months, a consistent presence of spinal cord septal cavitation (i.e., syringomyelia) was seen in MRI scans, and was confirmed by subsequent macroscopic examination. Interestingly, despite a comparable loss of motor function in this compression group, a variable extent of syringomyelia was seen between individual animals. We speculate that, as in human patients, substantial individual differences will be seen, and that much longer post-injury survival intervals will be needed for extensive syringomyelia to develop. Clinical data show that on average, a 5-year post-injury interval (range 6 months to 25 years) is needed for the development of syringomyelia in human patients with thoracic spinal cord injury (Carroll and Brackenridge, 2005).

Correlation between axonal loss and loss of neurological function

Overall, regardless of the severity of injury, there was a positive correlation between the degree of axonal loss and the extent of motor dysfunction. Subdividing the animals into those that displayed the ability to stand up and walk spontaneously, and those that were non-ambulatory (i.e., neurological score < 8), showed that overall bilateral axonal loss < 73% was associated with a paraplegic phenotype. The best correlation was seen between the loss of small- (0.5–2 μm) and medium-caliber (2–10 μm) axons in the lateral and ventral funiculi and loss of function. Despite a significant overall correlation between axonal loss and neurological dysfunction, a clear difference was seen between the distribution of axonal loss between the left and right halves of the spinal cord, particularly in the dorsal and lateral funiculus. We speculate that it could be the result of a partial lateral shift of the spinal cord during compression, and the resulting preferential injury at the site of maximum compression.

These data are in contrast to data from previous studies in a cat contusion model, which showed effective ambulatory function in some animals with up to 90% axonal loss. In addition, in the cat study a preferential loss of large-caliber myelinated axons in the ventral funiculi was seen in animals with ambulatory deficits (Blight, 1983). While the primary reasons for such discrepancies are not clear, they may reflect (1) interspecies differences in descending motor tract organization, (2) variability in the inter-segmental termination and organization of descending motor tracts, and (3) a variable degree of axonal sprouting from persisting axons below the level of injury. In addition, the differences in the velocity of spinal compression may play a role. In our study, a 3 cm/sec compression velocity was used, while the Blight study employed a weight-drop technique (Blight, 1983).

Thus a slower compression rate may cause more pronounced demyelinization.

Interestingly, in our current study animals in the 2.5-kg compression group demonstrated that axonal loss was not limited to areas directly impacted by the compression, but also included areas that displayed a relatively normal anatomical-histological picture (see Fig. 4F). We speculate that the development of local edema and the resulting secondary ischemia (Lemke and Faden, 1990; Lemke et al., 1987; Sasaki et al., 1978; Sharma and Olsson, 1990; Sharma et al., 1991) contributed to this remote type of axonal degeneration; these secondary changes were more pronounced after severe trauma (i.e., in the 2.5-kg compression group).

In contrast to the 2.5-kg compression group, which showed consistent paraplegia and was significantly different from the 2.0- and 1.5-kg groups, we were not able to detect significant differences between the 1.5- and 2.0-kg groups. It is likely that more sensitive tests such as video-based gait analysis will provide a more sensitive index of the functional deficits seen with these moderate types of injuries.

Continuing chronic inflammatory changes, but a lack of astrocytic scarring or schwannosis, was seen at chronic stages after spinal injury in minipigs

Immunostained sections taken from the epicenter of injury demonstrated the presence of inflammatory cellular elements, including IBA-1-postive microglia/macrophages and hypertrophic astrocytes. Although activated hypertrophic astrocytes were present, no typical astrocytic scar (defined as high-density astrocyte-filled areas) was present in sections taken 4 or 9 months after injury. Similarly, IBA-1-positive cells were present 4 to 9 months after injury, primarily surrounding and infiltrating cavities formed by axonal degeneration. The minipig prolonged inflammatory response is similar to the tissue healing seen in humans, which lasts 2–3 years, unlike the rodent inflammatory response to spinal cord injury, which lasts several weeks to months (Croul and Flanders, 1997; Dusart and Schwab, 1994). The presence of hypertrophic astrocytes, but the lack of astrocytic scar formation, in minipigs is similar if not identical to what has been described in human spinal cord specimens taken from patients at chronic stages of spinal cord injury. In these studies the presence of hypertrophic astrocytes was described; however, no typical astrocyte scar was identified (Norenberg et al., 2004). These authors' characterization included "… the extent of astrogliosis and 'scar' formation is relatively mild, at least in human(s)… a dense network of astroglial processes creating an impenetrable barrier is practically never seen." These observations are in contrast to the well-characterized astrocyte scar formation seen in rodents (Dijkstra et al., 2000; Frisen et al., 1995).

The presence of schwannosis (i.e., the accumulation of Schwann cells at the site of injury) has been described in spinal cord injury patients, particularly after penetrating injuries, with the Sevier-Munger stain (Bruce et al., 2000), and in the rat spinal contusion or demyelinization model in osmium-contrasted plastic sections, or after staining with Schwann cell–specific antibody (Schwann/2E; Jasmin et al., 2000; Keirstead et al., 2005). In our current study, the same antibody was used and confirmed a specific staining pattern in porcine dorsal roots (i.e., areas of normal distribution of Schwann cells). Staining of sections taken from areas considered positive for schwannosis in PPD-stained plastic sections were negative for the presence of Schwann cells. We speculate that instead these structures are primarily composed of fibroblasts (i.e., mesenchymal-derived), similar to the mesenchymal scar described in human spinal cord injury patients, primarily after a lacerating-type of injury (Berry et al., 1983; Norenberg et al., 2004).

Selection of the optimal minipig strain for studies of chronic spinal trauma

The progeny of cross-breeding Gottingen-Minnesota with domestic pigs, which were used in our study, are characterized by dense whole body hair growth. This soft skin "cushion" is a critical factor that makes these adult animals more resilient to chronic paraplegia by preventing the development of skin ulcers in the lower extremities. In contrast, despite our diligence, Yucatan minipigs, which have minimal to no body hair and a relatively thin epidermis, developed decubitus ulcerations with a very high incidence as soon as 1–2 days after injury (unpublished observation). The selection of minipig strains with whole-body hair growth is critical in minimizing the development of skin ulcerations in adult chronic paraplegic animals. Recently, a spinal weight-drop injury model using 3- to 5-week-old piglets (Yorkshire or "domestic" strain) was developed (Kuluz et al., 2010). To prevent the development of decubitus ulcers and to absorb body fluids in paraplegic animals, soft rubber mats covered with 2–3 inches of thin wood shavings were effective for 28 days of survival.

Development of spinal hyperreflexia in minipigs after spinal cord injury

Four of the eight animals that underwent severe trauma (the 2.5-kg compression group) continued to have an exacerbated muscle response to peripheral nociceptive stimuli 4–9 months after the initial injury. This was characterized by rapid muscle contraction that typically lasted for several seconds after applying the nociceptive stimulus. These animals also had a baseline increase in muscle tone (i.e., spastic hypertonia), affecting primarily extensor muscle groups. This observation is consistent with the development of spinal hyperreflexia or stimulus-evoked spasticity seen in patients with chronic spinal cord injury, which primarily reflects a loss of descending facilitatory input into segmental inhibitory interneurons (Adams and Hicks, 2005; Hiersemenzel et al., 2000).

Pros and cons of the utilization of the minipig spinal trauma model

The minipig spinal injury model represents an alternative model to already existing dog, cat, and non-human primate chronic spinal trauma models. It is characterized by a consistent, predictable, and stable neurological deficit after calibrated spinal trauma, as well as by the development of spinal cord histopathology comparable to changes seen in human patients. Several potential advantages and limitations associated with this porcine injury model include: (1) this minipig strain is able to tolerate severe neurological deficits and may be utilized for both acute and chronic treatment paradigms; (2) the technique for chronic intravenous drug delivery using chronically-placed intravenous jugular catheters and externally-mounted infusion pumps was developed and extensively tested (Usvald et al., 2010;

Utsugi et al., 2001). In addition, because the food reflex is particularly well developed in pigs, and the frequency of feeding cycles can be well pre-programmed, oral drug delivery may also be readily utilized, even in animals with chronic paralysis; (3) spinal cell transplantation or vector delivery techniques in minipigs using several injection devices was developed and successfully tested. This strain of animals was used to define the optimal spinal cell graft-dosing regimen for humans, and the design developed is currently being used in Phase I clinical trial in ALS patients receiving spinal grafts of human fetal neural precursors (Federici et al., 2009; Usvald et al., 2010); (4) a clear limitation of this porcine model is the lack of fine neuroanatomic/functional organization of the motor system, which is found in human and non-human primates. This model will not be suitable to detect the discrete therapeutic effects associated with the protection and/or sprouting of limited and functionally-distinct populations of motor axons.

Summary

We have developed and characterized a porcine model of chronic spinal cord contusion injury. We have demonstrated a stable neurological deficit after severe trauma which correlates with the development of spinal parenchymal septal cavitation at and around the injury epicenter. Histopathological analysis demonstrated the continuing presence of inflammatory cells up to 9 months after injury, but the lack of the typical astrocytic scar usually seen in rodent chronic spinal injury models. The neurological and spinal histological characteristics of this model appear to be similar to those seen in other large-animal spinal trauma models (primarily dogs), and in spinal cord-injured human patients. Accordingly, this model may represent an alternative spinal trauma model to the already existing dog, cat, and monkey models, to study new therapeutic approaches targeted to modulate the acute and chronic neurodegenerative changes associated with traumatic spinal cord injury.

Acknowledgments

This study was supported by a grant from the National Institutes of Health (NS051644 to M.M.), The Research & Development Operational Program funded by the ERDF (project No: 26220220127 from RDOP to M.M.), The Slovak Scientific Grant Agency VEGA (Project No: 2/0191/11 to Z.T.), The Ministry of Education, Youth and Sports of Czech Republic (Project No: 1M0538 to S.J., J.J., J.M.), The Technology Agency of Czech Republic (Project No: TA01011466 to S.J., J.J., J.M.) and The Institutional Research Plan of Academy of Sciences of Czech Republic (Project No: AV0Z50450515 to S.J., J.J., J.M.). Salary support (to G.S.) was provided by a Research Career Scientist Award from the Veterans Health Administration. The authors would like to thank Dr. Paul Reier (University of Florida, Department of Neuroscience, Mcknight Brain Institute, Gainesville) and Dr. Michele Basso (The Ohio State University) for their excellent advice in the preparation of this manuscript and Amber Millen (UCSD, Department of Anesthesiology) for editorial help.

Author Disclosure Statement

No competing financial interests exist.

References

Adams, M.M., and Hicks, A.L. (2005). Spasticity after spinal cord injury. Spinal Cord 43, 577–586.

Akhtar, A.Z., Pippin, J.J., and Sandusky, C.B. (2008). Animal models in spinal cord injury: a review. Rev. Neurosci. 19, 47–60.

Allen, A.R. (1911). Surgery of experimental lesion of spinal cord equivalent to crush injury of fracture dislocation of spinal column: a preliminary report. JAMA 57, 878–880.

Basso, D.M., Beattie, M.S., and Bresnahan, J.C. (1996a). Graded histological and locomotor outcomes after spinal cord contusion using the NYU weight-drop device versus transection. Exp. Neurol. 139, 244–256.

Basso, D.M., Beattie, M.S., Bresnahan, J.C., Anderson, D.K., Faden, A.I., Gruner, J.A., Holford, T.R., Hsu, C.Y., Noble, L.J., Nockels, R., Perot, P.L., Salzman, S.K., and Young, W. (1996b). MASCIS evaluation of open field locomotor scores: effects of experience and teamwork on reliability. Multicenter Animal Spinal Cord Injury Study. J. Neurotrauma 13, 343–359.

Berry, M., Maxwell, W.L., Logan, A., Mathewson, A., McConnell, P., Ashhurst, D.E., and Thomas, G.H. (1983). Deposition of scar tissue in the central nervous system. Acta Neurochir. Suppl. (Wien.) 32, 31–53.

Blight, A.R., and Decrescito, V. (1986). Morphometric analysis of experimental spinal cord injury in the cat: the relation of injury intensity to survival of myelinated axons. Neuroscience 19, 321–341.

Blight, A.R. (1983). Cellular morphology of chronic spinal cord injury in the cat: analysis of myelinated axons by line-sampling. Neuroscience 10, 521–543.

Bresnahan, J.C. (1978). An electron-microscopic analysis of axonal alterations following blunt contusion of the spinal cord of the rhesus monkey (*Macaca mulatta*). J. Neurol. Sci. 37, 59–82.

Bresnahan, J.C., King, J.S., Martin, G.F., and Yashon, D. (1976). A neuroanatomical analysis of spinal cord injury in the rhesus monkey (*Macaca mulatta*). J. Neurol. Sci. 28, 521–542.

Bruce, J.H., Norenberg, M.D., Kraydieh, S., Puckett, W., Marcillo, A., and Dietrich, D. (2000). Schwannosis: role of gliosis and proteoglycan in human spinal cord injury. J. Neurotrauma 17, 781–788.

Carroll, A.M., and Brackenridge, P. (2005). Post-traumatic syringomyelia: a review of the cases presenting in a regional spinal injuries unit in the north east of England over a 5-year period. Spine 30, 1206–1210.

Croul, S.E., and Flanders, A.E. (1997). Neuropathology of human spinal cord injury. Adv. Neurol. 72, 317–323.

Curtis, R., Green, D., Lindsay, R.M., and Wilkin, G.P. (1993). Up-regulation of GAP-43 and growth of axons in rat spinal cord after compression injury. J. Neurocytol. 22, 51–64.

Dietz, V., and Curt, A. (2006). Neurological aspects of spinal-cord repair: promises and challenges. Lancet Neurol. 5, 688–694.

Dijkstra, S., Geisert, E.J., Gispen, W.H., Bar, P.R., and Joosten, E.A. (2000). Up-regulation of CD81 (target of the antiproliferative antibody; TAPA) by reactive microglia and astrocytes after spinal cord injury in the rat. J. Comp. Neurol. 428, 266–277.

Dusart, I., and Schwab, M.E. (1994). Secondary cell death and the inflammatory reaction after dorsal hemisection of the rat spinal cord. Eur. J. Neurosci. 6, 712–724.

Ek, C.J., Habgood, M.D., Callaway, J.K., Dennis, R., Dziegielewska, K.M., Johansson, P.A., Potter, A., Wheaton, B., and Saunders, N.R. (2010). Spatio-temporal progression of grey and white matter damage following contusion injury in rat spinal cord. PLoS One 5, e12021.

Federici, T., Riley, J., Park, J., Bain, M., and Boulis, N. (2009). Preclinical safety validation of a stabilized viral vector direct

injection approach to the cervical spinal cord. Clin. Transl. Sci. 2, 165–167.

Fischer, F.R., and Peduzzi, J.D. (2007). Functional recovery in rats with chronic spinal cord injuries after exposure to an enriched environment. J. Spinal Cord Med. 30, 147–155.

Frisen, J., Haegerstrand, A., Risling, M., Fried, K., Johansson, C.B., Hammarberg, H., Elde, R., Hokfelt, T., and Cullheim, S. (1995). Spinal axons in central nervous system scar tissue are closely related to laminin-immunoreactive astrocytes. Neuroscience 65, 293–304.

Fukuda, S., Nakamura, T., Kishigami, Y., Endo, K., Azuma, T., Fujikawa, T., Tsutsumi, S., and Shimizu, Y. (2005). New canine spinal cord injury model free from laminectomy. Brain Res. Brain Res. Protoc. 14, 171–180.

Hagg, T., and Oudega, M. (2006). Degenerative and spontaneous regenerative processes after spinal cord injury. J. Neurotrauma 23, 264–280.

Hawryluk, G.W., Rowland, J., Kwon, B.K., and Fehlings, M.G. (2008). Protection and repair of the injured spinal cord: a review of completed, ongoing, and planned clinical trials for acute spinal cord injury. Neurosurg. Focus 25, E14.

Hiersemenzel, L.P., Curt, A., and Dietz, V. (2000). From spinal shock to spasticity: neuronal adaptations to a spinal cord injury. Neurology 54, 1574–1582.

Iwanami, A., Yamane, J., Katoh, H., Nakamura, M., Momoshima, S., Ishii, H., Tanioka, Y., Tamaoki, N., Nomura, T., Toyama, Y., and Okano, H. (2005). Establishment of graded spinal cord injury model in a nonhuman primate: the common marmoset. J. Neurosci. Res. 80, 172–181.

Jasmin, L., Janni, G., Moallem, T.M., Lappi, D.A., and Ohara, P.T. (2000). Schwann cells are removed from the spinal cord after effecting recovery from paraplegia. J. Neurosci. 20, 9215–9223.

Keirstead, H.S., Nistor, G., Bernal, G., Totoiu, M., Cloutier, F., Sharp, K., and Steward, O. (2005). Human embryonic stem cell-derived oligodendrocyte progenitor cell transplants remyelinate and restore locomotion after spinal cord injury. J. Neurosci. 25, 4694–4705.

Kuluz, J., Samdani, A., Benglis, D., Gonzalez-Brito, M., Solano, J.P., Ramirez, M.A., Luqman, A., De los Santos, R., Hutchinson, D., Nares, M., Padgett, K., He, D., Huang, T., Levi, A., Betz, R., and Dietrich, D. (2010). Pediatric spinal cord injury in infant piglets: description of a new large animal model and review of the literature. J. Spinal Cord Med. 33, 43–57.

Kwon, B.K., Hillyer, J., and Tetzlaff, W. (2010). Translational research in spinal cord injury: a survey of opinion from the SCI community. J. Neurotrauma 27, 21–33.

Lemke, M., and Faden, A.I. (1990). Edema development and ion changes in rat spinal cord after impact trauma: injury dose-response studies. J. Neurotrauma 7, 41–54.

Lemke, M., Demediuk, P., McIntosh, T.K., Vink, R., and Faden, A.I. (1987). Alterations in tissue Mg++, Na+ and spinal cord edema following impact trauma in rats. Biochem. Biophys. Res. Commun. 147, 1170–1175.

Lim, J.H., Piedrahita, J.A., Jackson, L., Ghashghaei, T., and Olby, N.J. (2010). Development of a model of sacrocaudal spinal cord injury in cloned Yucatan minipigs for cellular transplantation research. Cell Reprogram. 12, 689–697.

Noble, L.J., and Wrathall, J.R. (1989). Correlative analyses of lesion development and functional status after graded spinal cord contusive injuries in the rat. Exp. Neurol. 103, 34–40.

Norenberg, M.D., Smith, J., and Marcillo, A. (2004). The pathology of human spinal cord injury: defining the problems. J. Neurotrauma 21, 429–440.

Salgado-Ceballos, H., Guizar-Sahagun, G., Feria-Velasco, A., Grijalva, I., Espitia, L., Ibarra, A., and Madrazo, I. (1998). Spontaneous long-term remyelination after traumatic spinal cord injury in rats. Brain Res. 782, 126–135.

Sasaki, S., Schneider, H., and Renz, S. (1978). Microcirculatory disturbances during the early phase following experimental spinal cord trauma in the rat. Adv. Neurol. 20, 423–431.

Sharma, H.S., and Olsson, Y. (1990). Edema formation and cellular alterations following spinal cord injury in the rat and their modification with p-chlorophenylalanine. Acta Neuropathol. 79, 604–610.

Sharma, H.S., Winkler, T., Stalberg, E., Olsson, Y., and Dey, P.K. (1991). Evaluation of traumatic spinal cord edema using evoked potentials recorded from the spinal epidural space. An experimental study in the rat. J. Neurol. Sci. 102, 150–162.

Tarlov, I.M., and Klinger, H. (1954). Spinal cord compression studies. II. Time limits for recovery after acute compression in dogs. AMA Arch. Neurol. Psychiatry 71, 271–290.

Tarlov, I.M. (1954). Spinal cord compression studies. III. Time limits for recovery after gradual compression in dogs. AMA Arch. Neurol. Psychiatry 71, 588–597.

Tator, C.H. (2006). Review of treatment trials in human spinal cord injury: issues, difficulties, and recommendations. Neurosurgery 59, 957–982; discussion 982–957.

Usvald, D., Vodicka, P., Hlucilova, J., Prochazka, R., Motlik, J., Strnadel, J., Kucharova, K., Johe, K., Marsala, S., Scadeng, M., Kakinohana, O., Navarro, R., Santa, M., Hefferan, M.P., Yaksh, T.L., and Marsala, M. (2010). Analysis of dosing regimen and reproducibility of intraspinal grafting of human spinal stem cells in immunosuppressed minipigs. Cell Transplant. 19, 1103–1122.

Utsugi, R., Barth, R.N., Kitamura, H., Ambroz, J., Sachs, D.H., and Yamada, K. (2001). Tolerance across a two-haplotype, fully MHC-mismatched barrier induced in miniature swine renal allografts treated with a 12-day course of tacrolimus. Transplant Proc. 33, 101.

Vanicky, I., Urdzikova, L., Saganova, K., Cizkova, D., and Galik, J. (2001). A simple and reproducible model of spinal cord injury induced by epidural balloon inflation in the rat. J. Neurotrauma 18, 1399–1407.

Address correspondence to:
Martin Marsala, M.D.
Neuroregeneration Laboratory-0695
Department of Anesthesiology
University of California, San Diego
9500 Gilman Drive
San Diego, CA 92093-0695

E-mail: mmarsala@ucsd.edu